Earthquake Research Advances xxx (xxxx) xxx

Contents lists available at ScienceDirect

Earthquake Research Advances

journal homepage: www.keaipublishing.com/en/journals/earthquake-research-advances

Under the surface: Pressure-induced planetary-scale waves, volcanic lightning, and gaseous clouds caused by the submarine eruption of Hunga Tonga-Hunga Ha'apai volcano

David A. Yuen [a,b], Melissa A. Scruggs [c,*], Frank J. Spera [c], Yingcai Zheng [d], Hao Hu [d], Stephen R. McNutt [e], Glenn Thompson [e], Kyle Mandli [a], Barry R. Keller [f], Songqiao Shawn Wei [g], Zhigang Peng [h], Zili Zhou [i], Francesco Mulargia [j], Yuichiro Tanioka [k]

[a] Columbia University, Dept. of Applied Physics and Applied Mathematics, New York, NY, 10027, USA
[b] Ocean University of China, School of Computer Science and Marine Geosciences, Qingdao, 266100, China
[c] University of California, Santa Barbara, Dept. of Earth Science, 1006 Webb Hall, University of California, Santa Barbara, CA, 93106, USA
[d] University of Houston, Dept. of Earth and Atmospheric Sciences, Science & Research Bldg. 1, 3507 Cullen Boulevard, #312, Houston, TX, 77004, USA
[e] University of South Florida, School of Geosciences, Tampa, FL, USA
[f] Mission Beach, CA, USA
[g] Michigan State University, Dept. of Earth and Environmental Sciences, 288 Farm Ln Bldg, Room 207, East Lansing, MI, 48824, USA
[h] Georgia Institute of Technology, School of Atmospheric and Earth Sciences, North Avenue, Atlanta, GA, 30332, USA
[i] University of Southern California, Sonny Astani Dept. of Civil & Environmental Engineering, Kaprielian Hall, Los Angeles, CA, 90089-2531, USA
[j] University of Bologna, Dept. of Geological Sciences, Via Zamboni, 33, 40126, Bologna, Italy
[k] Hokkaido University, Division of Earth System Science, N10W5, Sapporo, Hokkaido, 060-0810, Japan

ARTICLE INFO

Keywords:
Hunga Tonga-Hunga Ha'apai
Atmospheric pressure wave
Tsunami wave
Volcanic lightning
Phreatoplinian eruption

ABSTRACT

We present a narrative of the eruptive events culminating in the cataclysmic January 15, 2022 eruption of Hunga Tonga-Hunga Ha'apai Volcano by synthesizing diverse preliminary seismic, volcanological, sound wave, and lightning data available within the first few weeks after the eruption occurred. The first hour of eruptive activity produced fast-propagating tsunami waves, long-period seismic waves, loud audible sound waves, infrasonic waves, exceptionally intense volcanic lightning and an unsteady volcanic plume that transiently reached—at 58 km—the Earth's mesosphere. Energetic seismic signals were recorded worldwide and the globally stacked seismogram showed episodic seismic events within the most intense periods of phreatoplinian activity, and they correlated well with the infrasound pressure waveform recorded in Fiji. Gravity wave signals were strong enough to be observed over the entire planet in just the first few hours, with some circling the Earth multiple times subsequently. These large-amplitude, long-wavelength atmospheric disturbances come from the Earth's atmosphere being forced by the magmatic mixture of tephra, melt and gasses emitted by the unsteady but quasi-continuous eruption from 0402±1–1800 UTC on January 15, 2022. Atmospheric forcing lasted much longer than rupturing from large earthquakes recorded on modern instruments, producing a type of shock wave that originated from the interaction between compressed air and ambient (wavy) sea surface. This scenario differs from conventional ideas of earthquake slip, landslides, or caldera collapse-generated tsunami waves because of the enormous (~1000x) volumetric change due to the supercritical nature of volatiles associated with the hot, volatile-rich phreatoplinian plume. The time series of plume altitude can be translated to volumetric discharge

* Corresponding author.
E-mail addresses: daveyuen@gmail.com (D.A. Yuen), thevolcanodoc@gmail.com (M.A. Scruggs), spera@geol.ucsb.edu (F.J. Spera), yzheng12@uh.edu (Y. Zheng), hhu5@central.uh.edu (H. Hu), smcnutt@usf.edu (S.R. McNutt), thompsong@usf.edu (G. Thompson), kyle.mandli@columbia.edu (K. Mandli), keller.barry@gmail.com (B.R. Keller), swei@msu.edu (S.S. Wei), zpeng@gatech.edu (Z. Peng), zilizhou@usc.edu (Z. Zhou), f.mulargia@gmail.com (F. Mulargia), tanioka@sci.hokudai.ac.jp (Y. Tanioka).

Production and Hosting by Elsevier on behalf of KeAi

https://doi.org/10.1016/j.eqrea.2022.100134
Received 20 February 2022; Received in revised form 10 March 2022; Accepted 12 March 2022

Please cite this article as: Yuen, D.A. et al., Under the surface: Pressure-induced planetary-scale waves, volcanic lightning, and gaseous clouds caused by the submarine eruption of Hunga Tonga-Hunga Ha'apai volcano, Earthquake Research Advances, https://doi.org/10.1016/j.eqrea.2022.100134

and mass flow rate. For an eruption duration of ~12 h, the eruptive volume and mass are estimated at 1.9 km^3 and ~2 900 Tg, respectively, corresponding to a VEI of 5–6 for this event. The high frequency and intensity of lightning was enhanced by the production of fine ash due to magma—seawater interaction with concomitant high charge per unit mass and the high pre-eruptive concentration of dissolved volatiles. Analysis of lightning flash frequencies provides a rapid metric for plume activity and eruption magnitude. Many aspects of this eruption await further investigation by multidisciplinary teams. It represents a unique opportunity for fundamental research regarding the complex, non-linear behavior of high energetic volcanic eruptions and attendant phenomena, with critical implications for hazard mitigation, volcano forecasting, and first-response efforts in future disasters.

1. Introduction

The eruption of Hunga Tonga-Hunga Ha'apai Volcano (HTHH) in mid-January 2022 was arguably the most violent volcanic eruption in the past 138 years. HTHH's first large eruption occurred on January 13, 2022 at 1520 UTC (14 January 4:20 local time), sending a plume of ash up to 20 km into the stratosphere. The cataclysmic eruption onset on January 15 at 0402 ± 1 UTC (~17:02 local time), with eruption intensity increasing drastically at ~0408 UTC (see Global Volcanism Program, 2022a) producing a plume that reached a maximum height of ~58 km—well within the mesosphere—by 0430 UTC (Bates and Carlowicz, 2022). These dramatic events, including attendant shock-waves, were captured by meteorological satellites, and were heard in New Zealand, Hawaii and in Alaska (Global Volcanism Program, 2022a). This eruption is on a par with other great eruptions including Pinatubo, Philippines in 1991 and Krakatoa in 1883 (Global Volcanism Program, 2022a) and exceeds the hitherto most powerful eruption known—the 180 CE ultra-plinian eruption of Taupo in New Zealand, which had an estimated plume height of ~50 km based on tephra dispersal (Walker, 1980). The eruption triggered a rare volcanogenic tsunami that caused loss of life and massive damage in the Kingdom of Tonga (Global Volcanism Program, 2022a,b,c). Historically, HTHH experienced at least two destructive, caldera-forming events prior to the January 2022 paroxysmal eruption, with the most recent dated at 1040–1180 CE (Cronin et al., 2017; Brenna et al., 2022). Magma recharge of the Hunga magmatic system culminating in caldera collapse evidently is a recurring phenomenon, at least in the Holocene. We refer the reader to Kusky (2022) for spectacular figures showing the eruption scenario and important geological information. Our paper differs from Kusky (2022) in that we focus on new technical details based on data analysis of seismic, acoustic, IR satellite imagery, volcanic lightning and geochemical data as well as scaling from geophysical, geochemical, volcanological and computational perspectives. We propose a first-order narrative of the climactic eruption, consistent with preliminary volcanological, infrasound, seismic, volcanic lightning, and tsunami observations and analyses that suggest the ingress of seawater played an important role in this violent,

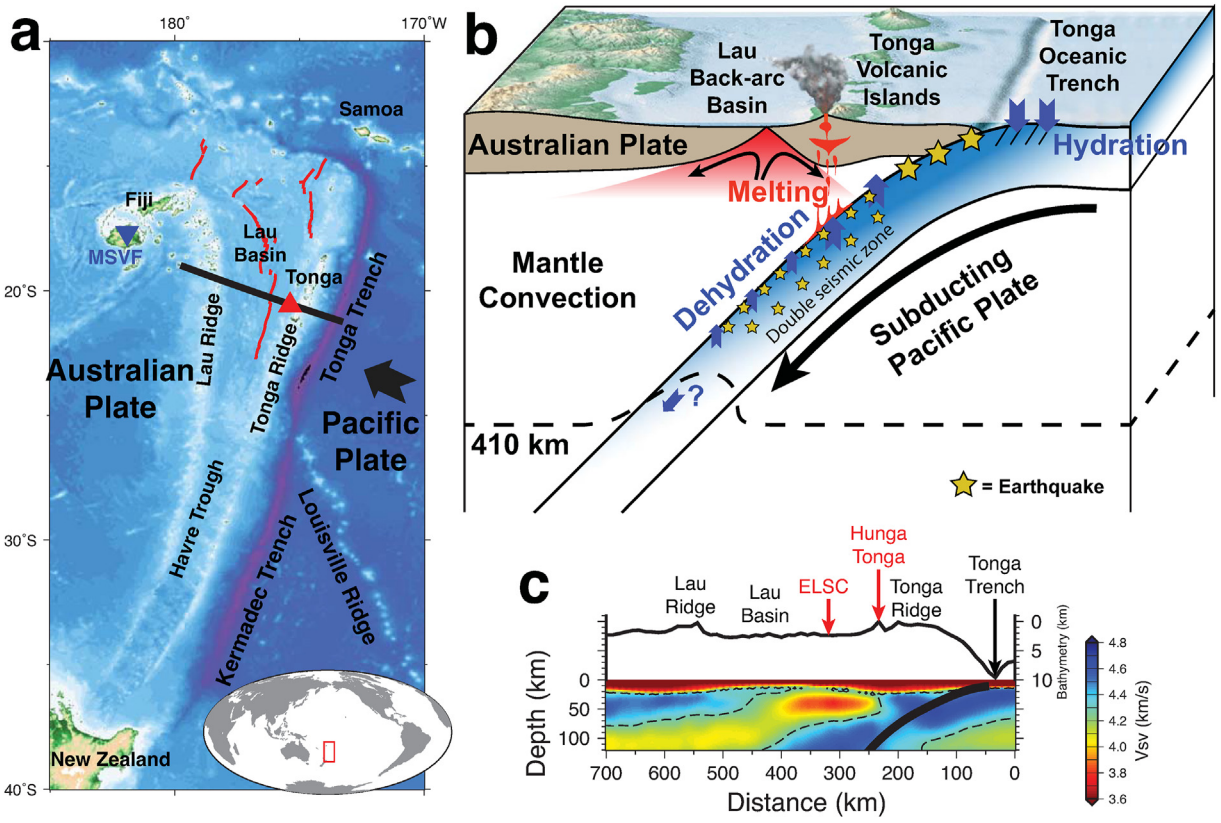

Fig. 1. **(a)** A map of the Tonga-Kermadec subduction system; inset shows this region on a global map. The black line indicates the cross section in panel **(c)**, whereas red lines illustrate back-arc spreading centers in the Lau Basin. The red triangle indicates the Hunga Tonga-Hunga Ha'apai volcano. **(b)** A schematic cartoon showing the Tonga-Lau subduction system. **(c)** A cross section of SV-wave velocity constrained by Rayleigh wave tomography (Wei et al., 2016). Bathymetry is plotted on top with vertical exaggeration. Hunga Tonga-Hunga Ha'apai and the East Lau Spreading Center (ELSC) are highlighted in red. Black bold curve indicates the Tonga slab surface according to the Slab1.0 model of Hayes et al. (2012).

phreatoplinian eruption. Fresh opportunities for future research and many challenges to multidisciplinary researchers abound.

2. Tectonic setting and background petrology of Hunga Tonga-Hunga Ha'apai volcano

The Tonga-Kermadec arc is an archetypical example of mature intra-oceanic island arc volcanism (Fig. 1a), and has served as a natural laboratory for evaluating subduction zone magmatism and the evolution of volcanic arcs (Smith and Price, 2006). Rapid (200–250 mm/yr) subduction of the Pacific Plate beneath the Indo-Australian plate, coupled with the onset of back-arc rifting at 2-5 Ma to form the adjacent Lau Basin (Bevis et al., 1995; Taylor et al., 2016), have resulted in a relatively thick ~20 km crustal column at the central Tonga Ridge (Contreras-Reyes et al., 2010; Brenna et al., 2022) that is home to one or more volumetrically significant, shallow magma reservoirs (Brenna et al., 2022). The mantle source for these arc magmas follows the interpretation of recent high-resolution seismic imaging of the Tonga Trench (Zheng et al., 2007; Li et al., 2019). Seismic velocity and attenuation images show that the decompression melting beneath the back-arc spreading system is much more extensive and intensive than the flux melting beneath the Tofua arc (Fig. 1c; Wei et al., 2015; Wei et al., 2016; Wei et al., 2018). The interactions between these two melting systems control the crustal structure as well as magma composition (Martinez and Taylor, 2002; Wei et al., 2015). Subduction of the Pacific oceanic lithosphere, including the hydrothermally-altered oceanic crust and uppermost partially serpentinized mantle, liberates volatiles at depth and triggers intermediate-depth earthquakes to form a double seismic zone (Fig. 1b; Wei et al., 2017). The volatiles trigger partial melting in the peridotitic mantle wedge region overlying the Wadati-Benioff zone (Smith and Price, 2006). Geochemical analyses of lavas erupted along this Tofua Volcanic (TVA) segment of the arc (Taylor et al., 2016) suggest that depleted mid-ocean ridge basalt (MORB) from the adjacent Lau Basin and pelagic sediments from the subducted slab also contribute to parental magma compositions (Smith and Price, 2006; Cooper et al., 2010). These magmas evolve by fractional crystallization and possibly ingestion of older wallrock during ascent through the crust, and undergo further compositional evolution in shallow storage reservoirs at 5–8 km depth accompanied by open-system magma recharge (Brenna et al., 2022), to produce basaltic andesites and andesites. Evidence for shallow magma reservoir growth, caldera resurgence, and vertical deformation since the early 2010s is shown by recently uplifted shore-platforms and fresh coral along the Hunga Tonga shoreline (Cronin et al., 2017; Brenna et al., 2022).

The island remnants of Hunga Tonga and Hunga Ha'apai are the highest points of HTHH, a ~2 km tall andesitic stratovolcano that lies ~67 km north-northwest of Tongatapu - the largest and most densely populated island in the Kingdom of Tonga (Cronin et al., 2017; Colombier et al., 2018). Eruptive activity was first recorded in 1912, but as the majority of the edifice is submarine, relatively little is known about the earlier eruptive history of HTHH (Bryan et al., 1972; Cronin et al., 2017). Subaerially exposed lavas of the main volcanic edifice are variably phenocrystic (2–40% pyroxene and plagioclase) basaltic-andesites and andesites (Brenna et al., 2022). On Hunga Ha'apai, lava flows are overlain by three sequences of highly-vesiculated, crystal-poor andesitic tephras, and topped by an andesitic welded ignimbrite produced during the caldera-forming eruption of 1040–1180 CE (Cronin et al., 2017; Brenna et al., 2022). Recently-erupted tephras from 2009 to 2014–15 have compositions very similar to older exposed tephra sequences, high inferred volatile contents (4.6–5.1 wt% H2O), and are slightly less evolved than the welded ignimbrite (Colombier et al., 2018; Brenna et al., 2022). For full geochemical and petrologic descriptions of earlier HTHH eruptive products, the reader is referred to Brenna et al. (2022).

The conceptual model of HTHH's magmatic system proposes that the magma source is an open-system shallow magma reservoir at 5–8 km depth that is compositionally and thermally buffered by the continuous or nearly-continuous recharge of homogeneous magmas (Brenna et al., 2022). Despite overlapping compositions between the caldera-forming welded ignimbrite and underlying tephras, a record of high-temperature mixing is preserved in the crystal cargo from caldera-forming events. As posited by Brenna et al. (2022), caldera-forming events at HTHH may be immediately triggered by mafic recharge. In between these large-scale events, the magma reservoir may be replenished by small amounts of well-homogenized melt, and volatiles accumulates in the magma as it crystallizes (Blake, 1984; Edmonds et al., 2022). These volatiles likely contributed to magmatic overpressure, triggering small, intra-caldera eruptions to maintain an equilibrium until sufficient volatiles had been concentrated to prime the HTHH magma reservoir (Caulfield et al., 2011; Edmonds et al., 2022; Geshi et al., 2022) for the paroxysmal January 15, 2022 eruption. Preliminary analyses of ashfall collected on January 15, 2022 suggest that an influx of volatile-saturated mafic magma had recently recharged the HTHH system, possibly triggering this paroxysmal event (Witze, 2022).

3. Provisional volcanology of the cataclysmic January 15, 2022 eruption

After seven years of inactivity, HTHH erupted on December 20, 2021 sending a plume of ash into the stratosphere (Global Volcanism Program, 2021). Eruptive activity continued intermittently for several weeks until January 13, 2022, when an episode of subaerial activity began at 1520 UTC, generating plumes of ash, steam, and gas that rose as high as 20 km. A 5 km-wide ash column was observed by Tongan geologists at 0530 UTC on 14 January (1830 local time; Global Volcanism Program (2022a). The subaerial activity was intermittent from 1143 to 1704 UTC, with plumes rising to ~15 km altitude. At 1820 UTC on January 14, a 10–15 min eruption produced an ash plume that rose to 14 km, and by the end of January 14, the middle third of the island that had been expanded over the previous two months was destroyed, relocating the vent to ~200 m b.s.l (Witze, 2022). We estimate that as much as 0.1 km^3 of magma may have been evacuated from the shallow magma storage reservoir between December 20, 2021 and the early afternoon of January 15, 2022. The removal of magma and a significant portion of the overlying edifice preceding the climactic January 15, 2022 event may have played a role in the particularly violent nature of the eruption, and should be better quantified in future studies.

On January 15, 2022, a large submarine phreatoplinian eruption at HTHH was initiated at ~0402 ± 1 UTC (~17:02 local time), based on infrasound and seismic data presented in Sections 4.2 and 4.3. By 0430 UTC the eruption plume had risen to a peak height of ~58 km (Bates and Carlowicz, 2022), and by 0603 UTC the plume umbrella was ~600 km wide (Global Volcanism Program, 2022a). Over the interval 0519–1000 UTC there were roughly 400 000 lightning strikes recorded by the GLD360 network (Global Volcanism Program, 2022a). Satellite imagery suggests plume heights were relatively sustained at >30 km from 0420 to 0850 UTC (Khlopenkov and Bedka, *unpublished footage*; Bates and Carlowicz, 2022), and that eruptive activity continued with varying intensities until ~1710 UTC. Residents on nearby Mango Island "fled to an area that was 30 m elevation, 700 m from the coast, and remained through the night as ash fell" (Global Volcanism Program, 2022c). Although initial reports are fragmentary, this suggests an eruption duration of circa 12 h. As of the time this manuscript was submitted, measurable volcanic activity at HTHH has ceased, and no notable seismic activity has occurred since January 24, 2022 (Global Volcanism Program, 2022b).

4. Summary of unusual observations and preliminary results

In this section we present a preliminary analysis of various signals—including lightning, infrasonics, eruptive plume heights, tsunami waves, and seismic waves—generated by this tsunamigenic eruption. Violently explosive, tsunamigenic eruptions are quite rare in the geologic record; this kind of eruption only happens at HTHH every ~1000 years or

so (Brenna et al., 2022). Large tsunamigenic earthquakes at subduction zones—such as the 2004 *M* 9.2 Sumatra, the 2011 *M* 9.1 Tohoku-Oki earthquake, and the 1964 *M* 9.2 Alaska earthquake—occur on relatively much shorter timescales. This event poses challenging questions for statisticians of rare events, as such eruptions do not conform to Gutenberg-Richter scaling, at least on humanly observable timescales. This eruption also excited Earth's atmosphere, producing gravity waves which circled the Earth multiple times, unprecedented amounts of volcanic lightning, and a shock wave which was heard as far away as Alaska (Adam, 2022; Global Volcanism Program, 2022).

4.1. Volcanic lightning observations

The HTHH eruption column produced a prodigious amount of volcanic lightning. The data we examined were summary data from the GDP360 instruments operated by Vaisala, Inc. The eruption the previous day, January 14, produced >190 000 flashes over 20 h (S. Ryan, *writt. comm.*). The stronger main eruption on January 15 produced >400 000 flashes in total with 200 000 flashes in the peak hour (S. Ryan, *writt. comm.*).

By conducting a frame-by-frame analysis of the same publicly available data (Churchill, *unpublished footage*) containing raw CG stroke counts by intensity, and interpolating the time of each stroke count from the underlain and correlated Himiwari-8 satellite footage, we obtained >700 000 sources (Fig. 2; Supplementary Table S1). During the strongest stage of the main eruption, the number of flashes was 80% of worldwide lightning during the most active hour! These observations are unprecedented.

We estimate that the first flashes occurred several minutes after eruption onset (Fig. 2; Supplementary Table S1), consistent with plume lightning elsewhere, such as Redoubt (Hoblitt, 1994; Behnke et al. 2013), Spurr (McNutt and Davis, 2000), and others. The lightning flashes expanded out from the source in a donut pattern as seen in videos (Churchill, *unpublished footage*; LightningOnDemand, *unpublished footage*), so many of the flashes occurred between 100 and 200 km from the volcano.

4.2. Volcanic infrasound observations

The January 15, 2022 eruption of HTHH produced the largest infrasound signals observed globally in 30 years. These signals were recorded on many stations worldwide, including all 53 arrays of the International Monitoring System (IMS) operated by the CTBTO (Brumfiel, 2022), but the relevant data is not publicly available at this time. Instead, we downloaded 1 Hz data from 117 infrasound and 584 barometric channels available from the Incorporated Research Institutions for Seismology Data Management Center (IRIS DMC), from January 13-20, 2022. After removing the instrument responses, we found that it was necessary to apply a 0.0001 Hz (10 000 s period) high-pass filter to fully resolve a characteristic *N*-shaped waveform of the blast wave from the main event. Kataoka et al. (*in submission*) and Amores et al. (*in submission*) identify this as a Lamb wave, which behaves like a surface wave propagating through the atmosphere. Filtering at higher frequencies causes the amplitude of the Lamb wave to be underestimated, and the shape to be distorted. The Lamb wave circled the globe in ~35.5 h and induced prominent seismic waves via air-ground coupling (Fig. 3) and meteotsunami.

After visually reviewing traces to eliminate noisy stations, we measured the maximum zero-to-peak amplitude of the Lamb wave at each remaining station (Fig. 4). It can be seen that the signal generally decays with distance, as expected. The peak Lamb wave amplitude at the closest station (757 km from HTHH) is 780 Pa, and the dominant wavelengths are 1–100 km. To estimate the strength of the signal at the source, we calculated reduced pressure. Reduced pressure is a metric used within the volcanic infrasound community to compare infrasound signals, and is an estimate of the pressure 1 km from the source. Assuming geometrical spreading like $1/\sqrt{r}$ (where r is the source-receiver distance), we estimate a reduced pressure of ~23 kPa (0.2 bars) by extrapolation back to 1 km (red line in Fig. 4). These pressures are so high that they imply the actual "source" was larger than 1 km (radius), and we consider 23 kPa a lower bound for reduced pressure. Long-wavelength infrasound at distances less than the thickness of the atmosphere would be expected to decay approximately like $1/r$, since wavefronts would be approximately hemispherical, like seismic body waves. Including this near field term, we estimate an upper bound of 170

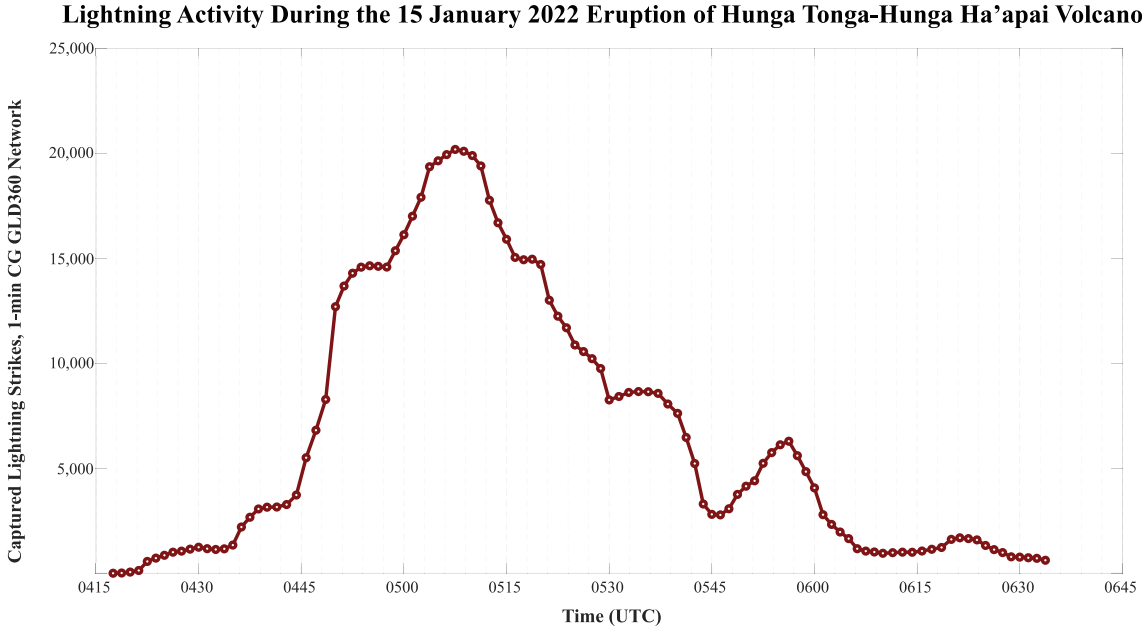

Fig. 2. Lightning activity during the January 15, 2022 eruption of Hunga Tonga-Hunga Ha'apai Volcano as a proxy for eruption intensity (Behnke and Bruning, 2015; Mendez-Harper et al., 2018). Data from unofficial 1-min CG records from the GLD360 dataset compiled by Churchill (*unpublished footage*).

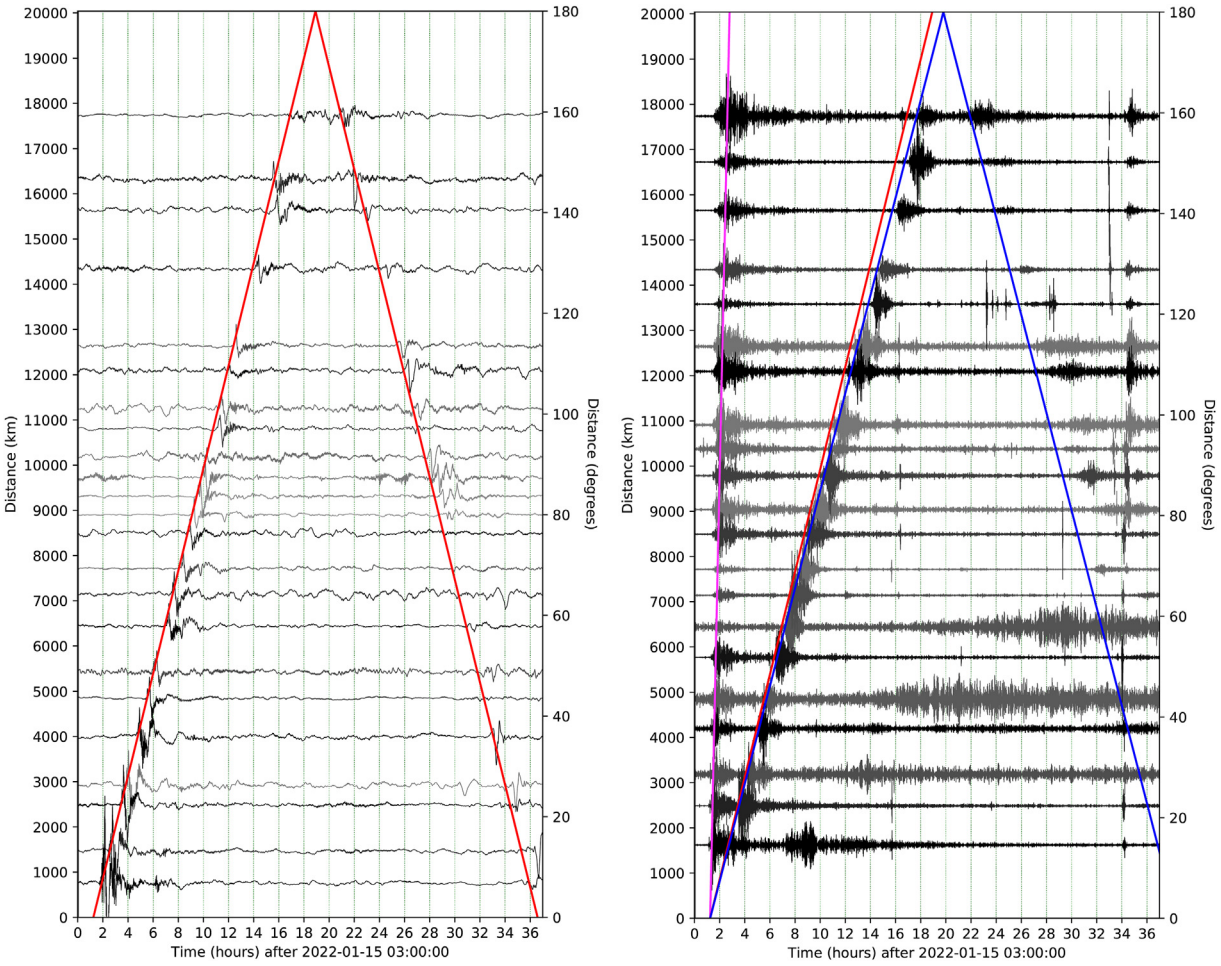

Fig. 3. Record sections of selected barograms (a), and seismograms (b). Barograms filtered from 10^{-4} to 10^{-1} Hz, show infrasound waves with a characteristic *N*-shaped-waveform, propagating around the globe at a speed of ~314 m/s (red line). We identify this as a Lamb wave. Seismograms are filtered from 10^{-3} to 10^{-1} Hz. Magenta line highlights surface waves at a speed of 3.9 km/s, and ground-coupled airwaves induced by the infrasound waves, propagating at ~300 m/s (blue line; red line shown for comparison). Barometric and seismic data are from IRIS DMC.

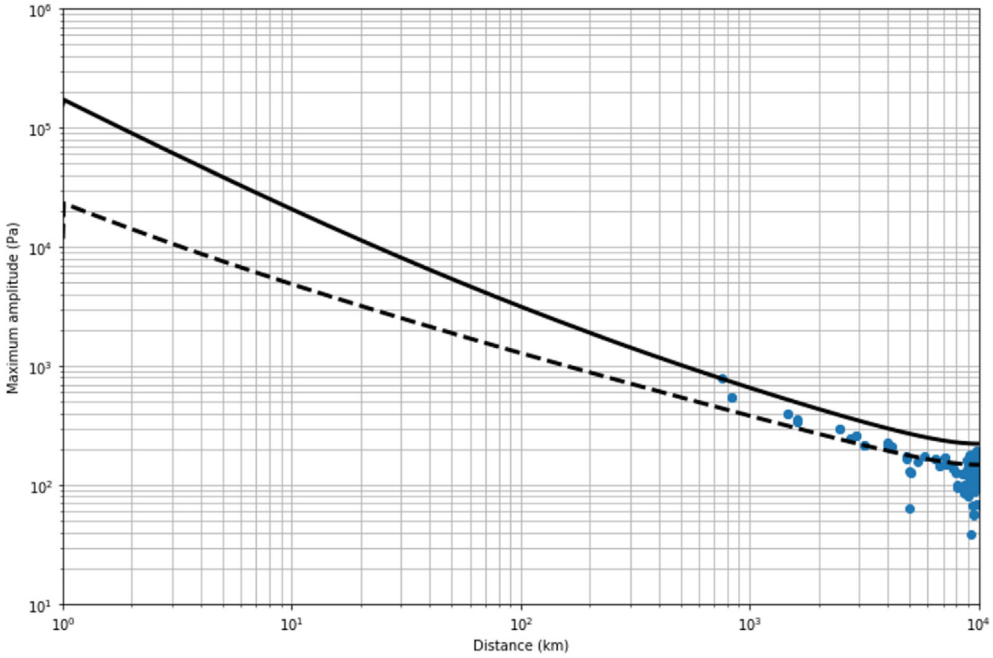

Fig. 4. Peak pressure amplitude of the Lamb wave vs. distance. Zero-to-peak pressure amplitude was measured on waveforms from 156 barometric stations available from the IRIS Data Management Center (DMC), after filtering between 0.0001 and 0.5 Hz. Extrapolating back to 1 km distance, assuming cylindrical wavefronts (dashed black line) suggests a reduced pressure of 23 kPa. Adding a near field term that represents spherical wavefronts in the first 100 km (solid black line) suggests a reduced pressure of 170 kPa.

kPa for reduced pressure. Comparison of these values with those from other eruptions (see Supplemental Appendix S2) suggests the January 15 HTHH eruption was in the VEI 5–6 range.

By manually picking the Lamb wave arrival at several dozen stations and performing a linear regression on arrival times versus distance, we determined a far-field speed of ~314 ± 3 m/s. This agrees with the theoretical predicted speed of 312 m/s for a Lamb wave (Bretherton, 1969). In the very near-field, the shockwave may have traveled much faster than this, perhaps reaching distant stations up to 1 min sooner. As best as we can determine, infrasound radiation indicative of an eruption began at ~0402 UTC ±1 min, and the Lamb wave emerged at ~0415 ± 2 min (consistent with the M_W 5.8 volcanic eruption), peaking around ~0429 ± 2 min.

4.3. Seismic observations and initial constraints on the source mechanism

Global seismic stations have widely recorded coherent seismic signals from the eruption (Fig. 5a). Consistent polarities over the full range of azimuths (Fig. 5b) indicate that these waves are not caused by shear faulting. Possible source mechanisms are likely to include vertical force, explosion, and implosion. The USGS reported a surface-wave magnitude 5.8 event for the eruption, with an origin time of 04:14:45 January 15, 2022 (UTC), located at 20.546°S, 175.390°E (USGS, 2022). Based on teleseismic waves, Poli and Shapiro (*in submission*) provides an estimation of VEI = 6 for the HTHH eruption, putting it among the largest volcanic eruptions ever recorded.

To better understand the source time functions of the HTHH eruption, here we directly stack the P-wave arrivals at teleseismic distances of 70–90°, where the seismic recordings are the densest, and coherent among different stations. This approach is somewhat similar to the direct stacking of teleseismic P waves for source time functions of deep-focus earthquakes (Houston and Vidale, 1994). Specifically, P-wave arrivals were picked and traces were aligned and stacked according to the picked times (Fig. 6a). The stacked ground velocity and displacement seismograms (Fig. 6b and c) show four seismic events: E−1, E−2, E−3, and E−4, with similar waveforms, suggesting episodic eruptive activities. The final event (E−4) is very close to E−3 in time, and is also considerably smaller in amplitude than the first three events. Within the first 300–400 s or so, a good correlation can be seen between the globally stacked seismograms (Fig. 7a and b) and the barometric pressure waveform recorded at a

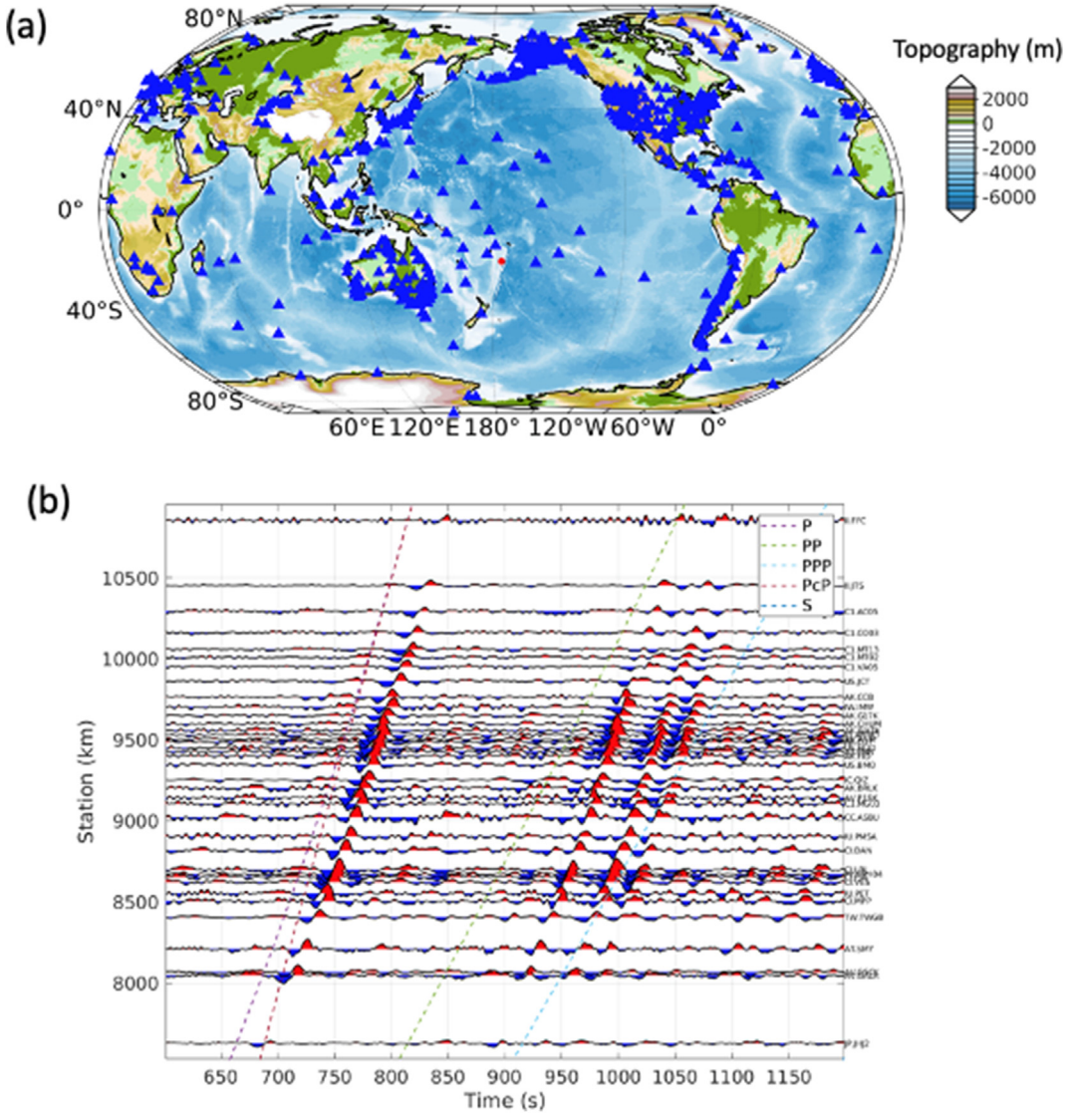

Fig. 5. Map of global seismic stations (a) and recorded waveforms of the HTHH eruption (b). In (a), blue triangles are stations and the red dot is HTHH volcano. In (b), the waveforms are vertical-component ground displacements, bandpass filtered within [10s 100s]. Theoretical traveltime curves, calculated using 1D Earth model (Yu et al., 2017) for the phases, P, PP, PPP, PcP, S, are shown.

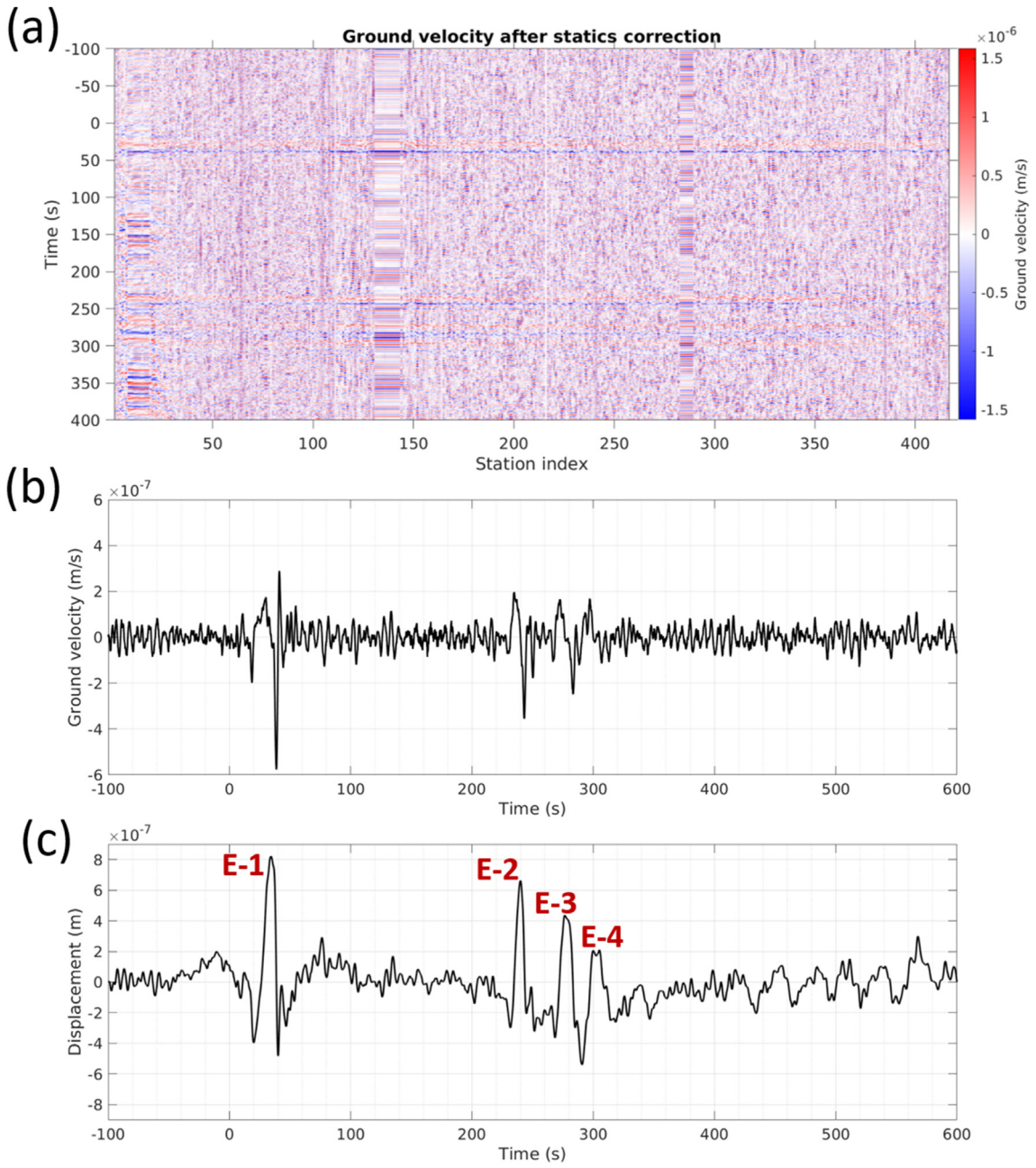

Fig. 6. (a) Ground velocity seismograms, high-pass filtered with a corner frequency of 0.01 Hz. Seismograms are aligned based on the picked P travel times. The seismograms are (b) stacked ground velocity; and (c) stacked ground displacement showing four episodic seismic events, E−1 to E−4.

nearby station in Fiji (Fig. 7c), which is ~757 km away from HTHH. This correlation confirms that the eruptive events generated both seismic signals and atmospheric pressure waves.

4.4. *Preliminary volcanological results*

Based upon the lightning detection record (Fig. 2; Churchill, *unpublished footage*; LightningOnDemand, *unpublished footage*) as a proxy for plume activity (Hoblitt, 1994; Lane and Gilbert, 1992), GOES-17 and Himawari-8 satellite imagery of 10.3 μm IR during the paroxysmal 15 January eruption (Khlopenkov and Bedka, *unpublished footage*; Bates and Carlowicz, 2022) and Global Volcanism Program reports (Global Volcanism Program, 2022a,b,c), peak and average volumetric discharge and mass flow, as well as total eruptive volume and mass can be estimated based on a scaling relationship between plume height and discharge (Carey and Bursik, 2000; see Appendix S4 for a more detailed explanation of our calculations). These are crude estimates since the role of external water has not been accounted for explicitly. The ingress of seawater enhanced the convective region of the volcanic plume (Koyaguchi and Woods, 1996; Mastin, 2007) as magma enthalpy converted seawater to buoyant steam. Based on the lightning proxy, satellite imagery and eye witness accounts, the eruption duration was circa 12 ±2 h. Infrasound analysis (Fig. 3), Lamb wave measurements (Fig. 4), and satellite footage (Khlopenkov and Bedka, *unpublished footage*; Bates and Carlowicz, 2022) suggest the eruption may have initiated as early as 0402 ± 1 UTC January 15, 2022, ~13 min before the M5.8 event origin time reported by USGS (2022). During the first 29 min of the eruption the plume grew to a colossal peak height of 58 km in the mesosphere, and then oscillated in the 45–50 km range until at least 0520 UTC (Khlopenkov and Bedka, *unpublished footage*; Bates and Carlowicz, 2022). For the following four hours or so the plume top decreased with some minor oscillations from ~37 km to ~28 km, and continued to decrease until the

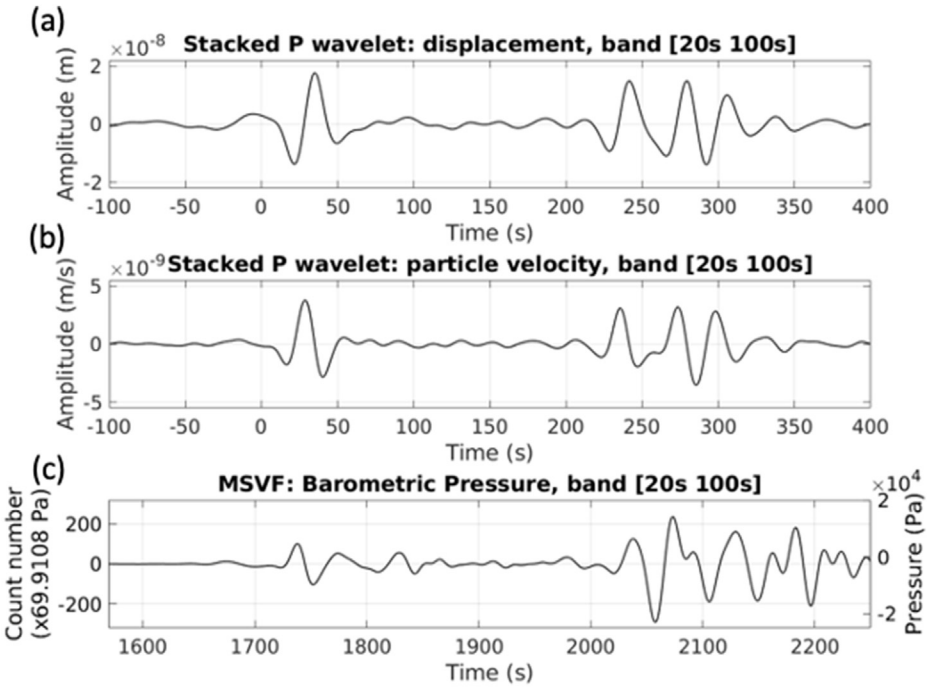

Fig. 7. Comparison of globally stacked seismograms recording ground displacement (a), ground velocity (b), and the barometric pressure record (c) at station MSVF in Fiji. All three waveforms are bandpass filtered within a period range [20s 100s].

eruption ceased (Khlopenkov and Bedka, *unpublished footage*; Bates and Carlowicz, 2022). We surmise that breaching of the magma chamber occurred at depth at 0402±1UTC, after which a bubbly, gas-laden and fragmenting magma made its way towards the surface. The exponential increase in eruption intensity at 0408 UTC could reflect the transition from surtseyan to subplinian activity, with the change to phreatoplinian activity marked by intense explosions beginning at 0414 ± 2 UTC and peaking at 0429 ± 2 UTC—the likely source of the incredibly large Lamb waves, tsunami, ground-coupled airwaves, meteo-tsunami, and colossal amounts of volcanic lightning.

Based on these first-order observations, peak volumetric discharge and mass flow rates of the volcanic plume are ~9×10^5 m^3/s and 1.3×10^9 kg/s, respectively, given a mean column density of 1500 kg/m^3 typical of phreatoplinian volcanic columns (e.g., Sparks et al., 1997). Integration of the plume height time series reconstructed from imagery gives a preliminary total eruptive volume of 1.9 km^3, corresponding to an eruptive mass of ~2 850 Tg. Explosive activity was aided by the relatively high concentration (~5 wt.% H_2O) of juvenile (magmatic) H_2O dissolved in the pre-eruptive melt, assuming that pre-eruptive wt.% H_2O is consistent with eruptive products from 2009 to 2014–2015 (Colombier et al., 2018; Brenna et al., 2022), which is a reasonable preliminary approximation. A high magmatic volatile content presumably increased the depth in the volcanic conduit at which magma fragmentation occurred, supercharging the later and shallower exchange of heat between already-fragmented magma and seawater, and affording the rapid flashing to steam with attendant enormous increase in volume. The conversion of pressure-volume work associated with the expansion to kinetic energy and vertically-directed momentum coupled to enhanced plume buoyancy enabled the vigorous plume to develop with associated atmospheric shock waves. As a crude estimate, if the mass fraction of seawater constituted 15% of the eruptive product, then the flashing of seawater from liquid to steam contributes ~2300 km^3 of volume expansion (Haar et al., 1984) when heated to magmatic temperatures. Indeed, a unique aspect of the HTHH eruption was the ingress of seawater (external, not magmatic water) and its phase change to a supercritical fluid. The *PV* work done pushing the atmosphere away from the eruptive vent constitutes an approximate mechanical energy of ~2×10^{17} J, which is in relatively good agreement with preliminary blast energies associated with atmospheric shock waves of 4–18 MT (see Appendix S2). Finally, the thermal energy of the eruption estimated at ~10^{19} J implies the conversion of thermal energy to blast energy was ~2%, well below the ideal Carnot cycle limit of ~80% for the conversion of heat to work. This is expected for the far-from-equilibrium dissipative phenomena associated with violent volcanic eruptions with attendant shock waves, tsunami and ground motions, and the violent expansion of heated seawater. The estimates made here are preliminary and remain to be refined, in some cases perhaps profoundly, as more complete analysis is made.

4.5. Tsunami observations and initial modeling results

The tsunami waves induced by the eruption were observed around the world (Adam, 2022; Kubota et al., *submitted*; Kataoka et al., *submitted*; Ramírez-Herrera et al., *submitted*; Tanioka et al., *in review*). We note that tidal data collected along the coast of Mexico (Ramírez-Herrera et al., *submitted*) and at La Jolla, CA (Fig. 8; Supplementary Table S4) showed strong signals for >100 h, as if the ocean was sloshing around. Similar measurements were made in Naples, which is close to the antipodal site from HTHH. The cause of this is not fully known, although it aligns with two different arrival times of waves: one at the normal gravity wave speed that most tsunami exhibit, and another arrival time corresponding to the acoustic waves that were also observed in the atmosphere (Fig. 3). These latter waves are similar to meteo-tsunami, waves caused by atmospheric pressure disturbances that are often also associated with resonance effects and also with bathymetric effects (Saito et al., 2021).

In terms of the modeling efforts of the tsunami, the major efforts from the National Tsunami Warning Center (NTWC) have centered around using the Deep Ocean Assessment and Reporting of Tsunamis (DART) buoy network in the Pacific to invert a set of Green's functions that could reconstruct the gravity wave components of the waves (the atmospheric signal was detected but was filtered out; NOAA Center for Tsunami Research, 2022). While this did represent the far-field gravity wave-based tsunami fairly accurately, the near-field will require significant computational resources to understand the true nature of the source

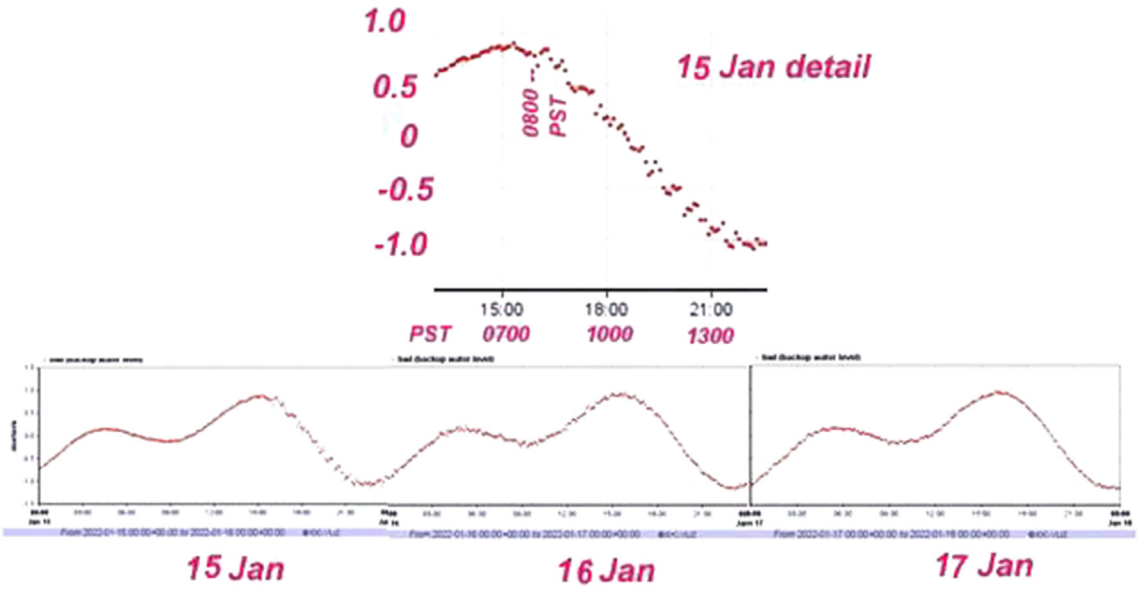

Fig. 8. Three-day record of La Jolla tidal station, at Scripps Pier. Tidal gauges are in a room in the southwestern corner of the building at the end of the pier. The vertical scale is in meters relative to the average value of each day's record. Mean sea level is at approximately zero, but varies slightly between records. The tsunami produced by the January 15 HTHH eruption arrived at La Jolla at approximately 0400 UTC on Jan 16, 2022 (0800 PST on January 15), with disturbances of tens of cm for many hours.

mechanisms for even the gravity wave. Several recent studies have modeled the initial tsunami waves as induced by atmospheric waves propagating at the speed of sound (i.e., the Lamb waves; e.g., Amores et al., *in submission*; Kubota et al., *in submission*), and subsequent tsunami as scattered waves by small islands in the Pacific Ocean.

5. Research opportunities

The cataclysmic January 15 eruption of HTHH presents a rare opportunity for researchers to explore new problems in volcanology, petrology and geochemistry, seismology, tsunamigenesis, infrasonics, atmospheric and climate science, physical chemistry, applied mathematics, and fluid dynamics and mechanics. As such, examining the events surrounding the HTHH eruption will require multidisciplinary collaborations. We illustrate this modus operandi in Fig. 9 below, and emphasize that the interdisciplinary effort needed to approach these problems is reflected in—but can certainly not be limited to—the composition of this writing team.

This study represents a first attempt at understanding the mechanics of this historic eruption, and we now wait for further, much-needed data—especially bathymetric measurements, petrologic and geochemical analyses—to be collected so that the scientific community can have a better understanding of these events. Geophysicists and seismologists will need to work together closely with volcanologists, igneous petrologists, geochemists, applied mathematicians, and physical chemists to better understand the syn-eruptive mechanics of phreatoplinian eruptions, as well as the pre-eruptive processes which primed HTHH for this historic eruption. This is necessary because the triggering mechanisms and thermochemical reactions of these violently explosive eruptions must be understood before developed seismic, tsunami, or atmospheric models can be properly reconciled and the implications for hazard analysis can be properly considered.

This rare volcanic event introduces new areas for fundamental research in volcanologically-induced tsunamigenesis, atmospheric physics, and wave generation. We present some possible avenues for exploration in these fields by raising questions for which answers are desperately needed, such as:

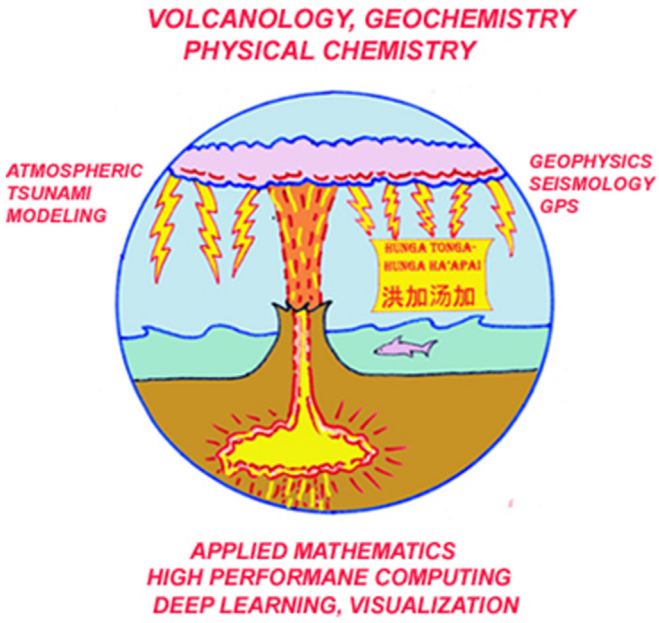

Fig. 9. An illustration of the real necessity for a multi-disciplinary team to understand the cataclysmic January 15, 2022 eruption of Hunga Tonga-Hunga Ha'apai Volcano. Seismologists alone cannot understand this unique phenomenon, and other disciplines are needed because an understanding of pre-eruptive volcanological events, as well as the physics and chemistry of the eruption itself, is inherently necessary to successfully address these novel research questions. Solutions to such complicated problems will require an increased demand in computational power and storage, and the implementation of applied mathematics, including machine learning.

1. Can a simplified 1-D tsunami excitation model be applied to tsunami waves generated by caldera collapse or explosion mechanisms?
2. What does the excitation model for these wave types look like?

3. Could localized 3-D models for caldera collapse (e.g., Tinti and Armgliato, 2003; Tinti et al., 2006) be used to model the HTHH eruption by using a not-mass-movement forcing model?
4. Could 3-D models for megathrust earthquakes that consider elastic as well as fluid dynamics (e.g., Saito and Furumura, 2009, or Saito and Kubota, 2020) be used to model the HTHH eruption?
5. What is the excitation distribution for the explosive component of a volcanic eruption when coupled with a landslide and/or caldera collapse? And how might nonlinear inversion models need to be adapted to account for these complex excitation mechanisms?
6. Can the complex seismic source time function be interpreted by the various magmatic and eruptive processes? Is a single-force model (Kanamori and Given, 1982) sufficient for modeling the seismic wavefield? Do we need a sequence of moment tensor sources and single-force sources to model the observed seismic fields? A joint inversion of seismic and tsunami waves (e.g., Ioki and Tanioka, 2011) should be carried out once tsunami data has been fully processed by Japanese researchers or NOAA, as such a modeling effort will provide us a great tool to understand the forces of the epic eruption of HTHH.
7. To what extent were the long-lived meteotsunami waves affected by the atmospheric pressure waves, as depicted in Fig. 10? And how might tsunami propagation calculations (e.g., Thurey et al., 2007; Schmidt et al., 2010) need to be adapted to account for such a mechanism?
8. What new knowledge can be gleaned from satellite observations of the eruption?
9. What thermochemical reactions are necessary to generate a far-reaching pressure wave?
10. How might complex wave interactions between the atmosphere and the ocean affect global wave propagation, and are these interactions globally recorded on tidal gauges and DART buoys?
11. Can detailed 3-D eruption column thermodynamic and dynamic models be used to quantify the role of seawater ingress and juvenile magmatic dissolved volatiles on the dynamics and electrostatic properties of tall volcanic plumes (Méndez Harper et al., 2020), such as the 58 km plume produced by HTHH?

The importance of understanding the source mechanism for this eruption cannot be understated. Even cutting-edge augmented reality (AR) tsunami-warning system efforts (https://www.zilizhou.com/tonga; Zhou, *unpublished dissertation proposal*) which can estimate arrival times and amplitudes at given locations through use of an app must still rely on equations that accurately capture the source mechanism. Thus, even the most advanced of warning systems is susceptible to holes in our scientific knowledge.

More than ever, this unprecedented eruption calls attention to the need for high-performance computing to describe these new phenomena, and address the above research questions and those that will undoubtedly follow. Scaling equations for the dynamics of volcanic eruptions (Woods, 2001) would complement current studies which examine how condensable gas jets present in submarine eruptions (Calahan and Dufek, 2020). Geoclaw tsunami modeling software developed by Berger et al. (2011) would require the use of parallel high-performance computing, and robust code needs to be generated to adapt the submarine landslide models of Heinrich et al. (2001) to account for the presence of a pressure wave in tsunamigenesis. To resolve these novel phenomena will require massive computational resources—we estimate ~100 million hours of high-performance computing time are needed, as well as a few hundred petabytes of cloud-based memory. We stress here that the computational requirements for this problem far exceed those required to model the 2004 Sumatra tsunami or the 2011 Tohoku-Oki tsunami, as there are multiple types of waves that must be analyzed and modeled, and the effects of inter-wave interactions and other non-linearities are currently unknown.

The opportunity to address novel phenomena in the Earth Sciences does not come around often, and we believe that this presents an ideal opportunity alongside traditional science HPC support for companies with a cloud computing structure—such as Microsoft, Amazon, and IBM—to support the sciences in their quest to understand the physics of events which had never before been recorded on modern instruments.

6. Concluding remarks

The destructive events of January 15, 2022 allow us to review the eruptive history of HTHH in a new light, as this very likely was a caldera-forming or caldera-modifying event. Large-scale explosive eruptions are more common at evolved dacitic-to-rhyodacitic systems, such as Pinatubo, Tofua, Krakatau, Rotorua, Raoul, and Santorini. However, repeated eruptions of pumice rafts in the South Pacific (Bryan et al., 2004; Taylor et al., 2016; Knafelc et al., 2020) and near Japan (Fiske et al., 2001; Geshi et al., 2022; Yoshida et al., *in review*) could imply these are more common than previously anticipated. Volcanoes of the Babuyan Archipelago pose a specific tsunamigenic threat to countries (and any highly populated urban centers) bordering the South China Sea, as Didicas and Babuyan volcanoes are capable of producing explosive (VEI ~4) phreatomagmatic eruptions, but have no permanent monitoring networks established (Paris et al., 2014; Terry et al., 2017). Further, the threat of submarine explosive eruptions and subsequent tsunami is not limited to the Pacific and Indian Ocean regions. The vent of Kick'em Jenny Volcano in the Lesser Antilles is located only ~150 m b.s.l. and the volcano has had numerous explosive eruptions since 1939, presenting significant hazards to Caribbean Island nations, the Americas, and countries around the Atlantic Rim (Harbitz et al., 2012; Day, 2015). This newest eruption of HTHH highlights the need to better understand mafic-to-intermediate stratocones at inter-oceanic arcs worldwide as, under the right conditions, they may produce cataclysmic, caldera-forming eruptions with global impact.

This momentous event also puts a spotlight on the nature of phreatoplinian eruptions (Houghton et al., 2015), and the novel type of tsunami waves they are capable of producing. We present a new mechanism from the introduction of supercritical fluids at the eruption site which caused their dramatic volumetric expansion and contributed to instabilities in magma flow (Wylie et al., 1999), producing excitations of the Earth's entire atmosphere, and generating unusually fast tsunami waves and unusually long-lived meteotsunami. This complex tsunamigenic scenario involves volcanology, petrology, and an understanding of eruption triggering mechanisms and the particular forces governing volcanic eruptions—an entirely different animal than traditional subduction zone earthquake tsunami generation models. The mechanisms of earthquakes are governed by nearly-instantaneous elastic and viscoelastic forces, whereas volcanic eruptions operate on timescales that are orders of magnitudes longer. This difference comes from the thermo-chemical evolution of multi-phase flow with supercritical Physico-chemical properties (Blundell and Blundell, 2009), such as viscosity and thermal expansivity. Thus, computational volcanology presents much greater difficulties than computational seismology. The statistics governing large tsunamigenic earthquakes are quite different from those describing tsunamigenic volcanic eruptions, and one must apply probability distributions to these types of events, which are much more difficult to evaluate than the well-defined Gutenberg-Richter relationship. This study represents a first attempt at understanding the mechanics of this historic eruption, and we now wait for further, much-needed data (bathymetric measurements, petrologic and geochemical analyses) to be collected so that the scientific community can have a better understanding of these events.

The cataclysmic January 15 eruption of HTHH presents a once-in-a-lifetime opportunity for young researchers to explore new, interdisciplinary problems in volcanology. Magmas that originated from Earth's mantle would later form the same eruption plume that traveled into Earth's mesosphere, initiating unprecedented atmospheric waves that traveled the globe. Truly, this was an event that requires the attention of

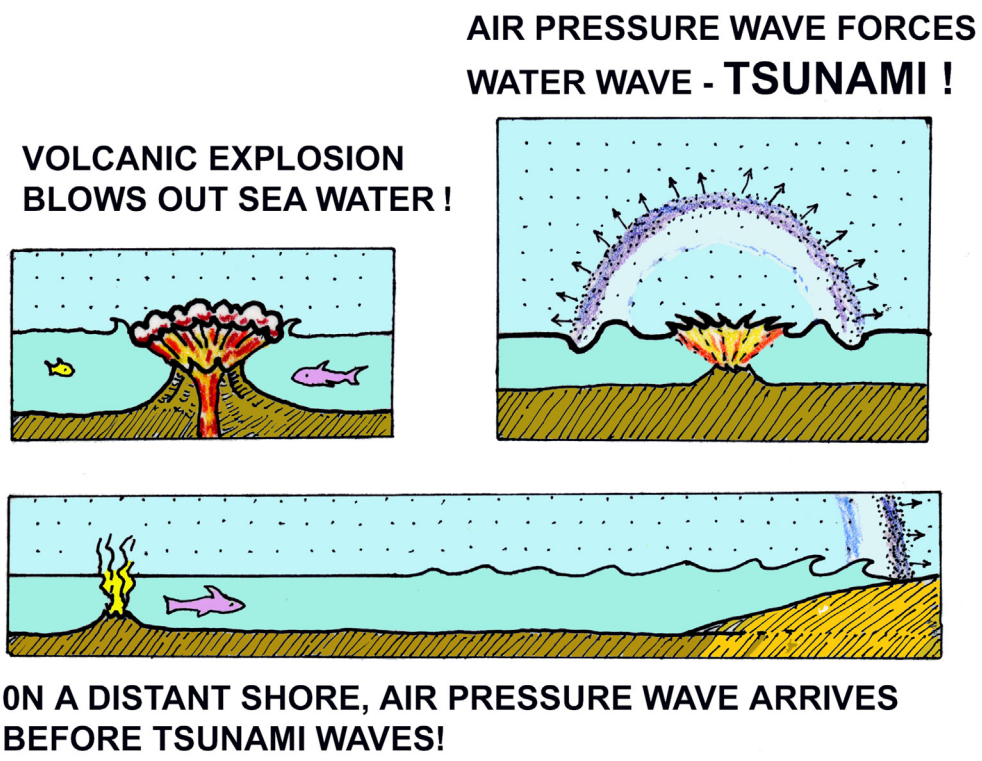

Fig. 10. Cartoon schematic illustrating how the eruption dynamics could produce tsunami waves with an unusual type of forcing from atmospheric pressure. These phenomena are very unusual and cannot be explained by conventional models that rely on the displacement of water by mass movement from earthquakes.

Earth scientists from all fields and backgrounds to understand its interdisciplinary nature. It may take many decades to flesh out the exact nature by which phreatoplinian eruptions generate fast-moving tsunami, atmospheric gravity waves, and disproportionately high eruption plumes. Nevertheless, we are very excited to see what discoveries the future holds.

Data and resources

Much of the data used to support the conclusions of this study were publicly available online, and were obtained from public social media accounts, footage publicly available on YouTube, and breaking news reports. All unpublished data were carefully vetted before consideration. Tidal measurements for the La Jolla, CA sea level station are publicly available at http://www.ioc-sealevelmonitoring.org/station.php?code=lajo. Green's function set inversions calculated by the National Tsunami Warning Center (NWTC) and related tsunami information are publicly available at https://nctr.pmel.noaa.gov/tonga20220115/. The facilities of the Incorporated Research Institutions for Seismology (IRIS) Data Management System, and specifically the IRIS Data Management Center, were used for access to the global seismic, infrasound, and barometric waveform and metadata used in this study. We downloaded data from network codes 2O, AK, AT, AU, AV, AZ, BK, C, C0, C1, CC, CH, CI, CM, CN, CU, CZ, DK, EI, G, GB, GE, GR, GS, GT, HV, IC, II, IM, IU, IW, JP, LD, LX, MN, MX, NA, N4, NL, NM, NU, NZ, OE, PL, PM, PS, PY, RO, SB, SC, SG, SS, TA, TX, UO, US, UU, WM, and WY, and these are publicly available at https://ds.iris.edu/ds/nodes/dmc/. The IRIS DMS is funded through the National Science Foundation and specifically the GEO Directorate through the Instrumentation and Facilities Program of the National Science Foundation under Cooperative Agreement EAR-0004370. We particularly relied upon data from the Global Seismographic Network (GSN). The GSN is a cooperative scientific facility operated jointly by the National Science Foundation (NSF) and the United States Geological Survey (USGS). The NSF component is part of NSF's SAGE facility, operated by IRIS under Cooperative Support Agreement EAR-1851048. A full citation list of the networks accessed and used in this study is given in Supplemental Item 6.

Declaration of competing interests

The authors declare that they have no known competing financial interests or personal relationships that could have appeared to influence the work reported in this paper.

Acknowledgements

We thank Professor Guoping Lu from Jinan University in Guangzhou, Professor Bob Zhu from Yunnan National Observatory in Kunming Yunnan, China, and Professor Hans Thybo from the Eurasia Institute of Earth Sciences for their thoughts on equations of state of supercritical fluids. We would also like to thank Dr. Shuxia Zhang and Dr. John Baumgardner for their interesting discussions concerning critical fluids, as well as Dr. Jed Brown from the University of Colorado, Dr. Xintong Xie from the Hainan Institute of Ocean Science and Technology, Josef Dufek from the University of Oregon, and E. Williams and R. Said for their discussions regarding this historic eruption. We thank the ERA editors and two anonymous reviewers for their valuable review comments and quick assistance during the review process. We thank Dr. Sara McBride and Dr. Janine Krippner for their mindful and considerate comments during the proofing process. This work was partially supported by US Department of Energy Grant DE-SC0019759 and National Science Foundation (NSF) Grants EAR-1918126, EAR-2027150, EAR-1925965, and OCE-1842989.

Appendix A. Supplementary data

Supplementary data to this article can be found online at https://doi.org/10.1016/j.eqrea.2022.100134.

References

Adam, David, 2022. Tonga volcano created puzzling atmospheric ripple. Nature 602, 497.

Amores, A., Monserrat, S., Marcos, M., Argüeso, D., Villalonga, J., Jordà, G. and Gomis, D. (in submission): numerical simulation of atmospheric Lamb waves generated by the 2022 Hunga-Tonga volcanic eruption. EarthARxiv. Preprint. https://eartharxiv.org/repository/view/3064/.

Bates, S., Carlowicz, M., 2022, 16 Feb. Tonga volcano plume reached the mesosphere. NASA Earth Observatory. https://earthobservatory.nasa.gov/images/14974/tonga-volcano-plume-reached-the-mesosphere. (Accessed 17 February 2022).

Behnke, S.A., Bruning, E.C., 2015. Changes to the turbulent kinematics of a volcanic plume inferred from lightning data. Geophys. Res. Lett. 42, 4232–4239. https://doi.org/10.1002/2015GL064199.

Behnke, S.A., Thomas, R.J., McNutt, S.R., Schneider, D.J., Krehbiel, P.R., Rison, W., Edens, H.E., 2013. Observations of volcanic lightning during the 2009 eruption of Redoubt Volcano. J. Volcanol. Geoth. Res. 259, 214–234.

Berger, M.J., George, D.L., LeVeque, R.J., Mandli, K.T., 2011. The Geo-Claw software for depth-averaged flows with adaptive refinement. Adv. Water Resour. 34, 1195–1206. https://doi.org/10.1016/j.advwatres.2011.02.016.

Bevis, M., Taylor, F.W., Schutz, B.E., Recy, J., Isacks, B.L., Helu, S., Singh, R., Kendrick, E., Stowell, J., Taylor, B., Calmant, S., 1995. Geodetic observations of very rapid convergence and back-arc extension at the Tonga arc. Nature 374 (6519), 249–251. https://doi.org/10.1038/374249a0.

Blake, S., 1984. Volatile oversaturation during the evolution of silicic magma chambers as an eruption trigger. J. Geophys. Res. 89 (B10), 8237–8244.

Blundell, S.J., Blundell, K.M., 2009. In: Concepts in Thermal Physics, *second ed.* Oxford University Press, New York, p. 496.

Brenna, M., Cronin, S.J., Smith, I.E.M., Pontesilli, A., Tost, M., Barker, S., Tonga'onevai, S., Kula, T., Rennie, V., 2022. Post-caldera volcanism reveals shallow priming of an intra-ocean arc andesitic caldera. Lithos 412–413, 106614. https://doi.org/10.1016/j.lithos.2022.106614.

Bretherton, F.P., 1969. Lamb waves in a nearly isothermal atmosphere. Q. J. R. Meteorol. Soc. 95, 754–757. https://doi.org/10.1002/qj.49709540608.

Brumfiel, G., 2022, 18 Jan. NASA Scientists Estimate Tonga Blast at 10 Megatons. NPR. https://www.npr.org/2022/01/18/1073800454/nasa-scientists-estimate-tonga-blast-at-10-megatons. (Accessed 26 January 2022).

Bryan, S.E., Cook, A., Evans, J.P., Colls, P.W., Wells, M.G., Lawrence, M.G., Jell, J.S., Greig, A., Leslie, R., 2004. Pumice rafting and faunal dispersion during 2001-2002 in the Southwest Pacific: record of a dacitic submarine explosive eruption from Tonga. Earth Planet Sci. Lett. 227, 135–154.

Bryan, W.B., Stice, G.D., Ewart, A., 1972. Geology, petrography, and geochemistry of the volcanic islands of Tonga. J. Geophys. Res. 77 (8), 1566–1585.

Calahan, R.C., Dufek, J., 2020. Explosive submarine eruptions: the role of condensable gas jets in underwater eruptions. J. Geophys. Res. Solid Earth 126 (2), e2020JB020969. https://doi.org/10.1029/2020JB0209691.

Carey, S., Bursik, M., 2000. Volcanic plumes. In: Sigurdsson, H., Houghton, B., Rymer, H., Stix, J., McNutt, S. (Eds.), The Encyclopedia of Volcanoes, pp. 113–141.

Caulfield, J.T., Cronin, S.J., Turner, S.P., Cooper, L.B., 2011. Mafic Plinian volcanism and ignimbrite emplacement at Tofua volcano, Tonga. Bull. Volcanol. 73, 1259–1277.

Churchill, W. [@ChurchillWx] (15 Jan 2022, 0908 UTC) "1-min CG lightning plot of #Tonga eruption" [Twitter post] https://twitter.com/ChurchillWx/status/1482278417466736651.

Colombier, M., Scheu, B., Wadsworth, F.B., Cronin, S., Vasseur, J., Dobson, K.J., Hess, K.-U., Tost, M., Yilmaz, T.I., Cimarelli, C., Brenna, M., Ruthensteiner, B., Dingwell, D.B., 2018. Vesiculation and quenching during surtseyan eruptions at Hunga Tonga-Hunga ha'apai volcano, Tonga. J. Geophys. Res. Solid Earth 123, 3762–3779.

Contreras-Reyes, E., Grevemeyer, I., Watts, A.B., Flueh, E.R., Peirce, C., Moeller, S., Papenberg, C., 2011. Deep seismic structure of the Tonga subduction zone: implications for mantle hydration, tectonic erosion, and arc magmatism. J. Geophys. Res. 116, B10103. https://doi.org/10.1029/2011JB008434.

Cooper, L.B., Plank, T., Arculus, R.J., Hauri, E.H., Hall, P.S., Parman, S.W., 2010. High-Ca boninites from the active Tonga Arc. J. Geophys. Res. 115, B10206. https://doi.org/10.1029/2009JB006367.

Cronin, S., Brenna, M., Smith, I.E.M., Barker, S., Tost, M., Ford, M., Tonga'onevai, S., Kula, T., Vaiomounga, R., 2017. New Volcanic Island unveils explosive past. Eos 98. https://doi.org/10.1029/2017EO076589.

Day, S., 2015. Volcanic tsunamis. In: Sigurdsson, H., Houghton, B., Rymer, H., Stix, J., McNutt, S. (Eds.), The Encyclopedia of Volcanoes, pp. 993–1009.

Edmonds, M., Liu, E.J., Cashman, K.V., 2022. Open-vent volcanoes fueled by depth-integrated magma degassing. Bull. Volcanol. 84, 28. https://doi.org/10.1007/s00445-021-01522-8.

Fiske, R.S., Naka, J., Iizasa, K., Yuasa, M., Klaus, A., 2001. Submarine silicic caldera at the front of the Izu-Bonin arc, Japan: voluminous seafloor eruptions of rhyolite pumice. GSA Bull. 113 (7), 813–824.

Geshi, N., Oikawa, T., Weller, D.J., Conway, C.E., 2022. Evolution of the magma plumbing system of Miyakejima volcano with periodic recharge of basaltic magmas. Earth Planets Space 74, 20. https://doi.org/10.1186/s40623-022-01577-7.

Global Volcanism Program, 2021. Report on Hunga Tonga-Hunga Ha'apai (Tonga). In: Sennert, S.K. (Ed.), Weekly Volcanic Activity Report, 22 December-28 December 2021. Smithsonian Institution and US Geological Survey.

Global Volcanism Program, 2022a. Report on Hunga Tonga-Hunga Ha'apai (Tonga). In: Sennert, S.K. (Ed.), Weekly Volcanic Activity Report. Smithsonian Institution and US Geological Survey, 12 January-18 January 2022.

Global Volcanism Program, 2022b. Report on Hunga Tonga-Hunga Ha'apai (Tonga). In: Sennert, S.K. (Ed.), Weekly Volcanic Activity Report, 19 January-25 January 2022. Smithsonian Institution and US Geological Survey.

Global Volcanism Program, 2022c. Report on Hunga Tonga-Hunga Ha'apai (Tonga). In: Sennert, S.K. (Ed.), Weekly Volcanic Activity Report, 2 February-8 February 2022. Smithsonian Institution and US Geological Survey.

Harbitz, C.B., Glimsdal, S., Bazin, S., Zamora, N., Lovholt, F., Bungum, H., Smebye, H., Gauer, P., Kjekstad, O., 2012. Tsunami hazard in the Caribbean: regional exposure derived from credible worst case scenarios. Continent. Shelf Res. 38, 1–23. https://doi.org/10.1016/j.csr.2012.02.006.

Haar, L., 1984. NBC/NRS STEAM TABLES: Thermodynamic and Transport Properties and Computer Programs for Vapor and Liquid States of Water in SI Units. CRC Press, Washington, DC.

Hayes, G.P., Wald, D.J., Johnson, R.L., 2012. Slab1.0: a three-dimensional model of global subduction zone geometries. J. Geophys. Res. Solid Earth 117 (B1), B01302. https://doi.org/10.1029/2011jb008524.

Heinrich, Ph, Piatanesi, A., Hebert, H., 2001. Numerical modelling of tsunami generation and propagation from submarine slumps: the 1998 Papua New Guinea event. Geophys. J. Int. 145, 97–111.

Hoblitt, R.P., 1994. An experiment to detect and locate lightning associated with eruptions of Redoubt Volcano. J. Volcanol. Geoth. Res. 62, 499–517.

Houston, H., Vidale, J., 1994. The temporal distribution of seismic radiation during deep earthquake rupture. Science 265, 771–774.

Houghton, B., White, J.D.L., Van Eaton, A.R., 2015. Phreatomagmatic and related eruption styles. In: Sigurdsson, H., Houghton, B., Rymer, H., Stix, J., McNutt, S. (Eds.), The Encyclopedia of Volcanoes, pp. 538–552.

Ioki, K., Tanioka, Y., 2011. Slip distribution of the 1963 Great Kurile Earthquake estimated from tsunami waveforms. Pure Appl. Geophys. 168, 1045–1052.

Kanamori, H., Given, J.W., 1982. Analysis of long-period seismic-waves excited by the May 18, 1980, eruption of Mount St Helens - a terrestrial monopole. J. Geophys. Res. 87 (NB7), 5422–5432.

Kataoka, R., Winn, S.D., and Touber, E. (in submission): Meteotsunamis in Japan associated with the Tonga eruption in January 2022. EarthARxiv. Preprint. https://eartharxiv.org/repository/view/3064.

Khlopenkov, K., Bedka, K., 2022, 20 Jan. Stereoscopic Geostationary Infrared Animation of the 15 Jan 2022 Hunga Tonga-Hunga Ha'apai Eruption [Video file], 20 Jan. Retrieved from. https://www.youtube.com/watch?v=kjP0cnLCwY8&t=1s.

Knafelc, J., Bryan, S.E., Gust, D., Cathey, H.E., 2020. Defining pre-eruptive conditions of the Havre 2012 submarine rhyolite eruption using crystal archives. Front. Earth Sci. 8, 310. https://doi.org/10.3389/feart.2020.00310.

Koyaguchi, T., Woods, A.W., 1996. On the formation of eruption columns following explosive mixing of magma and surface-water. J. Geophys. Res. 101 (B3), 5561–5574.

Kubota, T., Saito, T., and Nishida, K. (in submission): global fast-traveling tsunamis by atmospheric pressure waves on the 2022 Tonga eruption. EarthARxiv. Preprint. https://eartharxiv.org/repository/view/3090/.

Kusky, T.M., 2022. Déjà vu: might future eruptions of Hunga Tonga-Hunga ha'apai volcano be a repeat of the devastating eruption of Santorini, Greece (1650 BC)? J. Earth Sci. https://doi.org/10.1007/s12583-022-1624-2.

Lane, S.J., Gilbert, J.S., 1992. Electric potential gradient changes during explosive activity at Sakurajima volcano, Japan. Bull. Volcanol. 54, 590–594.

Li, L., Chen, Y.W., Zheng, Y., Hu, H., Wu, J., 2019. Seismic evidence for plume-slab interaction by high-resolution imaging of the 410 km discontinuity under Tonga. Geophys. Res. Lett. 46, 13678–13694.

LightningOnDemand (2022, 24 Jan) Lightning Strikes during Tonga Eruption [Video File]. Retrieved from https://www.youtube.com/watch?v=YD7Jf8F20Bg.

Mastin, L., 2007. A user-friendly one-dimensional model for wet volcanic plumes. Geochem. Geophy. Geosys. 8 (3). https://doi.org/10.1029/2006GC001455.

Martinez, F., Taylor, B., 2002. Mantle wedge control on back-arc crustal accretion. Nature 416 (6879), 417–420. https://doi.org/10.1038/416417a.

McNutt, S.R., Davis, C.M., 2000. Lightning associated with the 1992 eruptions of crater peak, mount Spurr volcano, Alaska. J. Volcanol. Geoth. Res. 102 (1–2), 45–65.

Méndez Harper, J.S., Cimarelli, C., Dufek, J., Gaudin, D., Thomas, R.J., 2018. Inferring compressible fluid dynamics from vent discharges during volcanic eruptions. Geophys. Res. Lett. 45, 7226–7235. https://doi.org/10.1029/2018FL078286.

Méndez Harper, J., Courtland, L., Dufek, Josef, McAdams, J., 2020. Microphysical effects of water content and temperature on the triboelectrification of volcanic ash on long time scales. J. Geophys. Res. Atmos. 125, e2019JD031498. https://doi.org/10.1029/2019JD031498.

NOAA Center for Tsunami Research Pacific Marine Environmental Laboratory (2022) Hunga Tonga-Hunga Ha'apai Volcano-Generated Tsunami, January 15, 2022 Main Event Page. https://nctr.pmel.noaa.gov/tonga20220115/. Accessed 15 Feb 2022.

Paris, R., Switzer, A.D., Belousova, M., Belousov, A., Ontowirjo, B., Whelley, P.L., Ulvrova, M., 2014. Volcanic tsunami: a review of source mechanisms, past events and hazards in Southeast Asia (Indonesia, Philippines, Papua New Guinea). Nat. Hazards 70, 447–470.

Poli, P. and N. Shapiro (in submission): Rapid characterization of large volcanic eruptions: measuring the impulse of the Hunga Tonga explosion from teleseismic waves. ESSOAr. Preprint. https://www.essoar.org/doi/10.1002/essoar.10510358.1.

Ramírez-Herrera, M.T., Coca, O., and Vargas-Espinosa, V. (in submission): tsunami effects on the Coast of Mexico by the Hunga Tonga-Hunga Ha'apai volcano eruption, Tonga. EarthARxiv. Preprint. https://eartharxiv.org/repository/view/3070/.

Saito, T., Furumura, T., 2009. Three-dimensional simulation of tsunami generation and propagation: application to intraplate events. J. Geophys. Res. 114, B02307. https://doi.org/10.1029/2007JB005523.

Saito, T., Kubota, T., 2020. Tsunami modeling for the deep sea and inside focal areas. Annu. Rev. Earth Planet Sci. 48, 121–145.

Saito, T., Kubota, T., Chikasada, N.Y., Tanaka, Y., Sandanbata, O., 2021. Meteorological tsunami generation due to sea-surface pressure change: three-dimensional theory and

synthetics of ocean-bottom pressure change. J. Geophys. Res.: Ocean 126, e2020JC017011. https://doi.org/10.1029/2020JC017011.

Schmidt, J., Piret, C., Zhang, N., Kadlec, B.J., Yuen, D.A., Liu, Y., Wright, G.B., Sevre, E.O.D., 2011. Modelling of tsunami waves and atmospheric swirling does with graphics processing unit (GPU) and radial basis functions (RBF). Concurr. Comp.-Pract. E. 22, 1813–1835. https://doi.org/10.1002/cpe.1507.

Smith, I.E.M., Price, R.C., 2006. The Tonga-Kermadec arc and Havre-Lau back-arc system: their role in the development of tectonic and magmatic models for the western Pacific. J. Volcanol. Geoth. Res. 156, 315–331.

Sparks, R.S.J., Bursik, M.I., Carey, S.N., Gilbert, J., Glaze, L.S., Sigurdsson, H., Woods, A., 1997. Volcanic Plumes. Wiley, Chichester, p. 590.

Tanioka, Y., Yamanaka, Y., and Nakagaki, T. (in review): characteristics of tsunamis observed in Japan due to the air wave from the 2022 Tonga eruption. ResearchSquare. Preprint. https://www.researchsquare.com/article/rs-1320093/v1.

Taylor, P.W., Mafi, K.S., 'Aho, P., 2016. Volcanic hazards and their management in the Kingdom of Tonga. In: Taylor, P.W. (Ed.), SPC Technical Bulletin SPC00017: Volcanic Hazards and Emergency Management in the Southwest Pacific, pp. 75–86.

Terry, J.P., Winspear, N., Goff, J., Hannah-Tan, P.H., 2017. Past and potential tsunami sources in the South China Sea: a brief synthesis. Earth Sci. Rev. 167, 47–61.

Thurey, N., Muller-Fischer, M., Schirm, S., Gross, M., 2007. Real-time breaking waves for shallow-water simulations. Computer Science. https://doi.org/10.1109/PG.2007.33.

Tinti, S., Armigliato, A., 2003. The use of scenarios to evaluate the tsunami impact of southern Italy. Mar. Geol. 199, 221–243.

Tinti, S., Pagnoni, G., Zaniboni, F., 2006. The landslides and tsunamis of the 30th of December 2002 in Stromboli analyzed through numerical simulations. Bull. Volcanol. 68 (5), 462–479.

USGS Earthquake Hazards Program (2022) M5.8 Volcanic Eruption - 68 Km NNW of Nuku'alofa, Tonga. https://earthquake.usgs.gov/earthquakes/eventpage/us7000gc8r/executive Accessed 15 Feb 2022.

Walker, G.P.L., 1980. The Taupo pumice: product of the most powerful known (ultraplinian) eruption? J. Volcanol. Geoth. Res. 8, 395–407.

Wei, S.S., Wiens, D.A., Zha, Y., Plank, T., Webb, S.C., Blackman, D.K., Dunn, R.A., Conder, J.A., 2015. Seismic evidence of effects of water on melt transport in the Lau back-arc mantle. Nature 518 (7539), 395–398. https://doi.org/10.1038/nature14113.

Wei, S.S., Zha, Y., Shen, W.S., Wiens, D.A., Conder, J.A., Webb, S.C., 2016. Upper mantle structure of the Tonga-Lau-Fiji region from Rayleigh wave tomography. G-cubed 17 (11), 4705–4724. https://doi.org/10.1002/2016gc006656.

Wei, S.S., Wiens, D.A., van Keken, P.E., Cai, C., 2017. Slab temperature controls on the Tonga double seismic zone and slab mantle dehydration. Sci. Adv. 3 (1), e1601755. https://doi.org/10.1126/sciadv.1601755.

Wei, S.S., Wiens, D.A., 2018. P-wave attenuation structure of the Lau back-arc basin and implications for mantle wedge processes. Earth Planet Sci. Lett. 502, 187–199. https://doi.org/10.1016/j.epsl.2018.09.005.

Witze, A., 2022. Why the Tongan volcanic eruption was so shocking. Nature 602, 376–378.

Woods, A.W., 2001. Explosive volcanic eruptions. In: Balmforth, N.J., Provenzale, A. (Eds.), Geomorphological Fluid Mechanics. Springer Verlag, pp. 188–208.

Wylie, J.J., Voight, B., Whitehead, J.A., 1999. Instability of magma flow from volatile-dependent viscosity. Science 285, 1883–1885.

Yoshida, K., Tamura, Y., Sato, T., Hanyu, T., Usui, Y., Chang, Q., Shigeaki, O. (in review): variety of the drift pumice clasts from the 2021 Fukutoku-Oka-no-Ba eruption, Japan. EarthARxiv. Preprint. https://eartharxiv.org/repository/view/2878/.

Yu, C., Zheng, Y., Shang, X., 2017. Crazyseismic: a MATLAB GUI-based software package for passive seismic data preprocessing. Seismol Res. Lett. 88 (2A), 410–415.

Zheng, Y., Lay, T., Flanagan, M.P., Williams, Q., 2007. Pervasive seismic wave reflectivity and metasomatism of the Tonga Mantle Wedge. Science 316, 855–869.

Zhou, Zili, 2022. Immersive Computing for Coastal Engineering. University of Southern California. Unpublished PhD Dissertation Proposal. https://zilizhou.com/tonga.